Electron scattering from gaseous SF_6: Comparing calculations with experiments

F. A. Gianturco[a)]
Max-Planck-Institut für Strömungsforschung, Bunsenstraße 10, D 37073 Göttingen, Germany and Department of Chemistry, Texas A&M University, College Station, Texas 77843-3255

R. R. Lucchese
Department of Chemistry, Texas A&M University, College Station, Texas 77843-3255

(Received 24 October 2000; accepted 6 December 2000)

The dynamical observables associated with low-energy electron scattering from SF_6 molecules in the gas-phase, e.g., elastic differential cross sections, integral elastic cross sections and momentum transfer cross sections, are computed using quantum methods and describing the full interaction between the molecule and the impinging electron without empirical parameters. The above quantities are obtained over an energy interval ranging from a few meV up to 100 eV and the results are compared with the available experiments. Various aspects of the theoretical method employed are analyzed in relation to their agreement with the experimental data discussed in this work. © *2001 American Institute of Physics.* [DOI: 10.1063/1.1343900]

I. INTRODUCTION

It has been known for many years now that electron–molecule collisions, and in general the physical interpretation of electron-driven chemical phenomena, bears great importance on our detailed knowledge of environmental processes and of the plasma processing of materials.[1,2] Since electrons, even at fairly low energies, are capable of perturbing the electronic structure of the molecules of the ambient gas, they are thus able to initiate a very broad variety of reactive events.

The processes observed are seen to exhibit greatly varying flux distributions among the possible open channels at the considered energies and such variations clearly depend on the microscopic structures of the molecular ambient gases.[3] The level of detailed interpretation of the quantum elementary events which becomes necessary in order to explain what is being observed, or to predict how a given molecular species is likely to behave, has then to be provided by flexible, realistic and computationally robust theoretical models that can handle such a variety of processes.

On the other hand, and especially when one deals with nonlinear polyatomic molecules in the ambient gas, our current knowledge of even the simpler among the scattering observables is still fairly limited to a few-atom species and to few-electron structures. Even then, the many possible inelastic channels that lead to rovibrational and electronic excitations or to ionization/fragmentation by electron impact are still very little known and rather insufficiently predicted by most of the current theoretical methods.[4] It is therefore still important, from the point of view of testing and assembling microscopic quantum models, to at least reproduce the behavior of the elastic channels for increasingly more complicated molecules and to be able to generate for them total elastic cross sections and elastic angular distributions which satisfactorily describe the corresponding experimental findings.

It is the aim of the present work to perform this type of comparison for the evaluation of elastic differential cross sections (DCS) of gaseous SF_6 molecules which have been recently measured over a broad range of energies,[5,6] and to compute the corresponding momentum transfer cross sections (MTCS) over the same range of energies (from 0.5 eV up to 100 eV). We have also obtained the integral elastic cross sections (ECS) and compared them with the recently available experimental data.[6] The present calculations intend to revisit some of our earlier work on the title system,[7] to extend it by testing the effects of different basis set which describe the target and by generating new dynamical data to compare with the latest experiments.[5,6] The following section briefly outlines our computational procedure, already described many times before,[4] while Sec. III will report the computational details and look at the numerical convergence of our results. The present DCS will be compared with the experimental data in Sec. IV, while Sec. V reports our comparison between computed and measured elastic and total cross sections. Our final conclusions are given in Sec. VI.

II. THE SCATTERING EQUATIONS

A. Single center expansions

Resonant and nonresonant low-energy scattering of electrons from polyatomic targets has been studied in our group, over the years, at various levels of sophistication for the description of (i) the electronuclear structure of the target molecule, (ii) the interaction forces between the bound particles and the impinging electron, and (iii) the dynamical formulation of the quantum scattering equations.[8]

We have used an *ab initio*, parameter-free approach

a)Author to whom correspondence should be addressed. Dipartimento di Chimica, Citta-Universitaria, 00185, Rome (I); Fax: +39-06-499/3305; electronic mail: fagiant@caspur.it

 © 2001 American Institute of Physics

Downloaded 06 Jan 2009 to 143.248.103.32. Redistribution subject to AIP license or copyright; see http://jcp.aip.org/jcp/copyright.jsp

starting with the target nuclei being kept fixed at their equilibrium geometry, i.e., with their motion during the scattering process decoupled from the other variables. This simplifying scheme is known as the fixed nuclei (FN) approximation,[4] and it greatly reduces the dimensionality of the coupled scattering equations for the dynamics. In our implementation of such equations, any arbitrary three-dimensional function describing a given electron, either one of the N bound electrons or the scattering electron, is expanded around a single-center (SCE) usually taken to be the center of mass of the global $(N+1)$ electron molecular structure

$$F^{p\mu}(r,\hat{\mathbf{r}}|\mathbf{R})=\sum_{l,h} r^{-1} f_{lh}^{p\mu}(r|\mathbf{R}) X_{lh}^{p\mu}(\hat{\mathbf{r}}). \tag{1}$$

In the above SCE representation $F^{p\mu}$ refers to the μth element of the pth irreducible representation (IR) of the point group of the molecule at the nuclear geometry $\mathbf{R}$. The angular functions $X_{lh}^{p\mu}(\hat{\mathbf{r}})$ (Ref. 9) are symmetry-adapted angular functions.

Once all the bound and continuum wave functions have been expanded using Eq. (1), then the quantum scattering equations will give us a way of evaluating the unknown radial coefficients of Eq. (1) for the $(N+1)$th continuum electron by using the SCE radial quantities for the occupied target MOs,

$$\left[\frac{d^2}{dr^2}-\frac{l(l+1)}{r^2}+2(E-\epsilon_\alpha)\right] f_{lh}^{p\mu\alpha}(r|\mathbf{R}) = 2\sum_{l'h'\beta'} \int dr' V_{lh,l'h'}^{p\mu\alpha\beta}(r,r'|\mathbf{R}) f_{l'h'}^{p\mu,\beta}(r'|\mathbf{R}), \tag{2}$$

where E is the collision energy $E=k^2/2$ and ϵ_α is the electronic eigenvalue for the αth asymptotic state. The $(p\mu)$ indices label the specific μth component of the pth IR that belongs to the αth electronic target state (initial state) coupled to the excited state indexed by β. The coupled partial integro-differential equations (IDEs), Eq. (2), contain the kernel of the potential operator V which is a sum of diagonal and nondiagonal terms that in principle can fully describe the electron–molecule interaction during the collision. The near-HF wave function from a single determinant (SD) SCF calculation can be used to represent the bound target electrons, thus reducing the sum on the r.h.s. of Eq. (2) to a single state α only. This simplification gives the static-exchange (SE) representation of the electron-molecule interaction for the chosen electronic target state (usually the ground state) at the nuclear geometry $\mathbf{R}$.

The numerical solutions of Eq. (2) will produce the relevant K-matrix elements which will in turn yield the elastic (rotationally summed) differential cross sections, obtained for scattering by randomly oriented molecules by averaging the scattering amplitude $f(\hat{k}\cdot\hat{r}|\alpha,\beta,\gamma)$ over all the angular values,[10]

$$\frac{d\sigma}{d\Omega}(\hat{k}\cdot\hat{r})=\frac{1}{8\pi^2}\int |f(\hat{k}\cdot\hat{r}|\alpha,\beta,\gamma)|^2 d\alpha \sin\beta d\beta d\gamma. \tag{3}$$

A more convenient formulation of the above quantity can be had by writing[10]

$$\frac{d\sigma}{d\Omega}(\hat{k}\cdot\hat{r})=\sum_L A_L P_L(\cos\theta), \tag{4}$$

with θ being now the center-of-mass angle from the impinging direction of $\hat{k}$. The coefficients A_L have been given explicitly before[9,10] and will not be repeated here. The interested reader can refer to the above work for the details.

B. Interaction forces

For a target which has a closed-shell electronic structure, as in the present case, with $n_{\rm occ}=N/2$ doubly occupied orbitals φ_i, and when only a single state is included in the expansion of Eq. (2), the potential is the static-exchange potential of the form,

$$V_{\rm SE}(\mathbf{r})=\sum_{\gamma=1}^{M}\frac{Z_\gamma}{|\mathbf{r}-\mathbf{R}_\gamma|}+\sum_{i=1}^{n_{\rm occ}}(2\hat{J}_i-\hat{K}_i), \tag{5}$$

where $\hat{J}_i$ and $\hat{K}_i$ are the usual local static potential and the nonlocal exchange potential operators, respectively. The index γ labels one of the M nuclei located at the coordinate $\mathbf{R}_\gamma$ in the center-of-mass, molecular frame of reference (MF).

At lower energies the neglect of important polarization effects can cause the wrong energy behavior and the incorrect magnitude computed cross sections. Neglecting polarization can also significantly alter the energy and width of the shape resonances that may exist at lower energies. This difficulty could be met in principle by the inclusion of additional pseudostates in the expansion of the target wave function,[11] however, they significantly increase the computational complexity of solving the scattering equations, especially in the case of larger molecular targets as in the present example. We have therefore tested over the years an alternative computational option that takes advantage of the findings of density functional theory (DFT) on the behavior of correlation effects.[12]

In particular, to include the full electron–molecule potential the long-range polarization terms and the short-range dynamical correlation effects, we have implemented a local, energy-independent model potential, $V_{\rm CP}(r)$, which has been discussed before.[9,13] Briefly, the $V_{\rm CP}$ model potential contains a short-range correlation contribution, $V_{\rm corr}$, which is smoothly connected to a long-range polarization contribution, $V_{\rm pol}$. The short-range term is obtained by defining an average dynamical correlation energy of a single electron within the formalism of the Kohn and Sham variational orbitals representing the bound electrons. The functional derivative of such a quantity with respect to the SCF N-electron density of the molecular target provides a density functional description of the required short-range correlation term (for a general discussion of DFT methods, see Parr and Yang[12]). The long-range part of $V_{\rm CP}$ is obtained by first constructing a model polarization potential, $V_{\rm pol}$, which asymptotically agrees with the potential obtained from the static dipole polarizability of the target in its ground electronic state. This corresponds to including the dipole term in the second-order perturbation expansion of the polarization potential. In the

Downloaded 06 Jan 2009 to 143.248.103.32. Redistribution subject to AIP license or copyright; see http://jcp.aip.org/jcp/copyright.jsp

case of SF_6, a molecule of octahedral symmetry, we have improved somewhat empirically on the spherical nature of the α_0-driven term by taking the experimental polarizability value of 44.134 a_0^3 and distributing it over the seven atomic centers of the target. Thus, the contribution on the S atom was 16.198 a_3^3 and that from each F atom was 4.656 a_0^3. The overall symmetry of such an anisotropic distribution will therefore follow the various irreducible representations of the molecular point group.

Since, in a general case, the long-range contribution, $V_{\rm pol}$, does not exactly match the short-range correlation, $V_{\rm corr}$, at any given value of r, one needs to define a procedure to connect it to $V_{\rm pol}$. The value of $r_{\rm match}$ is obtained by first computing the SCE of both contributions and then finding the smallest r where the two radial functions for $l=0$ intersect. This has been, in fact, what we found in many cases to be the more realistic empirical choice.[15,17] This intersection (or closest approach of the two potentials in the cases where the two $l=0$ potentials do not intersect) then defines $r_{\rm match}$. A modified $V_{\rm pol}$ is then given by

$$V_{\rm pol}^{\rm match}(\mathbf{r}) = V_{\rm pol}(\mathbf{r}) + \sum_{lm} C_{lm} r^{-\lambda} Y_{lm}(\theta,\phi). \tag{6}$$

The C_{lm} coefficients are determined by making the $V_{\rm pol}^{\rm match}$ exactly equal to $V_{\rm corr}$ at $r=r_{\rm match}$. The exponent λ is a function of l such that $\lambda(l)=6,5,6$ for $l=0,1,2$ and $\lambda(l)=l+2$ for $l\geqslant 3$. The latter function is chosen so that the term added to $V_{\rm pol}$ has the functional form of the first term neglected in the perturbation expansion of $V_{\rm pol}$. As has been discussed previously,[14] a switching function is then used to smoothly switch between $V_{\rm pol}^{\rm match}$ and $V_{\rm corr}$ in the region of match. When $V_{\rm CP}$ is added the $V_{\rm SE}$, the resulting potential is the static-exchange-correlation-polarization (SECP) potential.

III. NUMERICAL AND CONVERGENCE TESTS

One of the technical problems when carrying out numerical treatments involving basis set expansions is that of acquiring some quantitative information on the level of convergence which has been achieved with the specific choices made for the target basis set expansion, the partial wave expansion for the continuum electron and the multipolar expansion for the electron–molecule interaction. In this section we will give the details of our treatment and some examples of the sensitivity of our results on the convergence parameters mentioned above.

As mentioned before, we carried our SECP calculations within the FN approximation and the SF bond length was kept fixed at its experimental value of 1.560 23 Å. In our earlier work on the same system[7] the bound molecular orbitals (MO's) of the target SF_6 molecule were obtained using a 6-311G($2d$,$2p$) basis set expansion equivalent to a triple-zeta quality of the valence orbitals plus (p,d) polarization functions on the sulfur and fluorine atoms. The total electronic energy that we found for that wave function was −993.786 672 a.u. In the present calculations we decided to use three different basis set expansions in order to see their effect on the computed dynamical observables. Thus, we employed first an aug-cc-pVDZ expansion, which yielded a total energy of −994.085 655 866 a.u., fairly close to the earlier calculations.[7] We then enlarged the size of the basis set by moving on to an aug-cc-pVTZ basis that yielded an improved state of −994.317 846 582 a.u. We further enlarged the expansion by carrying out calculations with an aug-cc-pVQZ basis set which produced a total electronic energy value of −994.377 225 208 a.u. These three basis sets will be denoted as the DZ, TZ, and QZ basis sets, respectively, in the remainder of the paper. All the corresponding occupied MO's were used in our calculations after subjecting them to a single-center expansion. The radial numerical grid used in the present study contained 1792 points from the origin to 14 a.u. The minimum step size was 1.2×10^{-5} a.u. near the S atom. Except where noted, the corresponding multipolar expansion of the potential was kept at $l_{\rm max}=40$, as we had already found before to produce converged K-matrix values.[7] The continuum electron expansion was also carried out up to $l_{\rm max}=40$ for the largest contributing partial wave.

TABLE I. Computed integral cross sections, at two representative energies, using the different basis sets discussed in the main text.

E (eV)	Basis set	ECS (Å^2)	MTCS (Å^2)
5.0	DZ	26.241	17.772
5.0	TZ	26.132	17.759
5.0	QZ	26.071	17.763
30.0	DZ	28.815	18.626
30.0	TZ	29.294	18.859
30.0	QZ	29.397	18.924

In Table I we show, for two energies in the range of energies examined in this work, the computed values of the total elastic cross sections (ECS) and of the momentum-transfer cross sections (MTCS) using the three different target expansions of the present work. We have also tested these effects for other energy values and the general behavior was found to be the same. We see that the change in going from the TZ to the QZ expansion is of less than 1%, thereby suggesting that we can consider the QZ level of basis set expansion as producing essentially converged results. These convergence effects could also be seen by comparing the computed DCS at the same energies shown in Table I. The latter dynamical observable is in fact a rather sensitive quantity and should tell us even more directly on the quality of the basis set selected.

The results of the comparison are shown in Fig. 1, where we report the two sets of angular distributions at the two collision energies of 5.0 and 30.0 eV. The panel on the left shows the cross sections on a log scale while the panel on the right gives them on a linear scale in order to show better the low-intensity region. The dot-dashed lines report the calculations with the DZ basis set while the dashed lines refer to the TZ basis set expansion. The results from the largest expansion with the QZ basis set are given by solid lines. One clearly sees from that figure that the DCS shapes and values are very similar by all three basis sets and that the TZ and QZ expansions produce DCS values that are essentially converged.

Another interesting point where convergence tests should be carried out is the one concerned with the widths

Downloaded 06 Jan 2009 to 143.248.103.32. Redistribution subject to AIP license or copyright; see http://jcp.aip.org/jcp/copyright.jsp

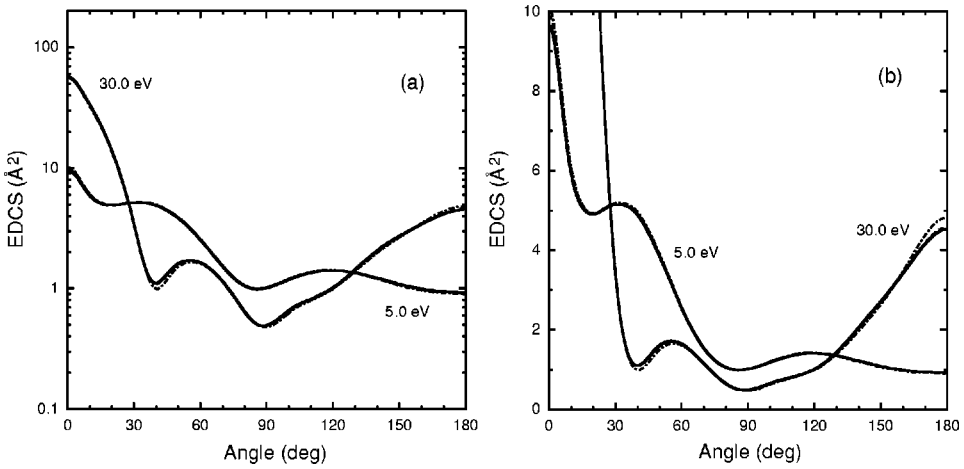

FIG. 1. Computed elastic differential cross sections (EDCS) at two different collision energies and as a function of different basis set expansion. Dotted–dashed lines, DZ basis set; dotted lines, TZ basis set; solid lines, QZ basis set. (a) Intensities on a log scale. (b) Intensities on a linear scale.

and positions of the single-channel resonances observed in the e-SF_6 scattering system. In order to consider those effects, we have examined some of the more prominent resonances already discussed and analyzed before[7] and have repeated the calculations with the three different basis set expansions selected in the present work. The results are reported in Table II, where we give the energy positions (eV) and the widths Γ (also eV) of the shape resonances as a function of the basis set expansions for the target MO's. All calculations where carried out with $l_{\max}=40$, with the exception of the A_{1g} low-energy resonance where several l values were tested, as we shall further discuss below.

The results reported in Table II indicate that, although the target orbital expansion plays a role in affecting the resonance features, the changes are all rather modest and invariably indicate that the results with the QZ expansion are essentially converged in both energy position and width value. With respect to the results obtained earlier,[7] a comparison our own data of Table I in that paper with the present calculations indeed show that the basis set used there produced similar features for the three resonances of T_{1u}, T_{2g}, and E_g symmetry that exhibited (E_R,Γ_R) values within 2%–3% of the present data. We further add here two resonances at higher energy which were not discussed in Ref. 7: The T_{1g} resonance at 60 eV and the T_{1u} resonance at 10 eV, both appearing also in the behavior of the integral cross sections that we shall discuss later on. The latter shape resonance was also discovered in the earlier work on the sulfur 1s photoionization in SF_6 carried out by some of us[15] where a single-particle resonance at a photoelectron energy of 57 eV, with a width of 8.5 eV, was observed. The attachment process to a neutral target obviously now shifts its location and modifies its width but the microscopic physical origin remains the same.

TABLE II. Computed single particle resonance parameters for the e^--SF_6 system as a function of target basis set expansion and of partial wave expansion.

Symmetry	Basis set	$l_{\max}$	E_R (eV)	Γ_R (eV)
A_{1g}	DZ	40	2.885	0.162
	TZ	40	3.418	0.136
	QZ	40	3.531	0.133
$T_{1u}(1)$	DZ	40	8.903	0.922
	TZ	40	9.529	0.946
	QZ	40	9.658	0.948
T_{2g}	DZ	40	12.950	1.005
	TZ	40	13.354	1.152
	QZ	40	13.429	1.175
E_g	DZ	40	28.419	1.765
	TZ	40	28.940	1.876
	QZ	40	29.018	1.907
T_{1g}	DZ	40	58.820	19.183
	TZ	40	58.975	19.343
	QZ	40	58.999	19.342
$T_{1u}(2)$	DZ	40	69.642	15.132
	TZ	40	69.905	15.260
	QZ	40	69.958	15.246
A_{1g}	QZ	25	3.887	0.246
	QZ	30	3.721	0.063
	QZ	35	3.710	0.058
	QZ	40	3.531	0.133

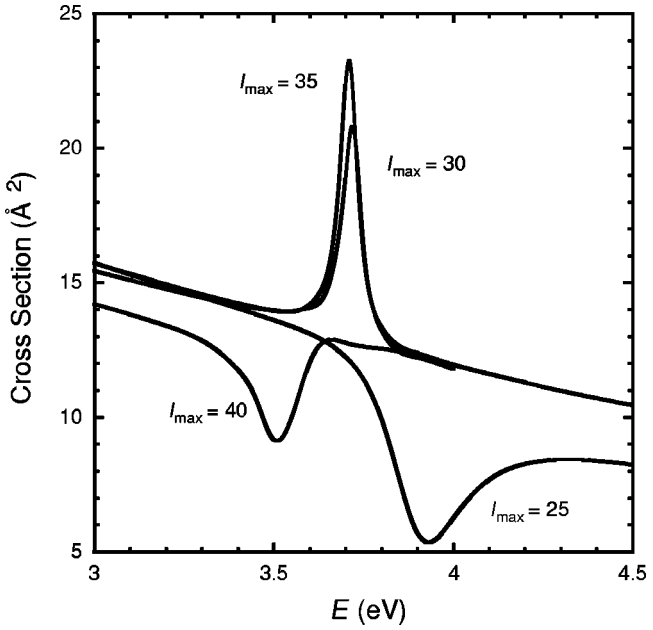

FIG. 2. Behavior of the elastic integral cross sections as a function of energy around the position of the A_{1g} resonant feature. The four different curves refer to the four indicated values of the maximum angular momentum employed in the partial wave expansion of the continuum electron.

Downloaded 06 Jan 2009 to 143.248.103.32. Redistribution subject to AIP license or copyright; see http://jcp.aip.org/jcp/copyright.jsp

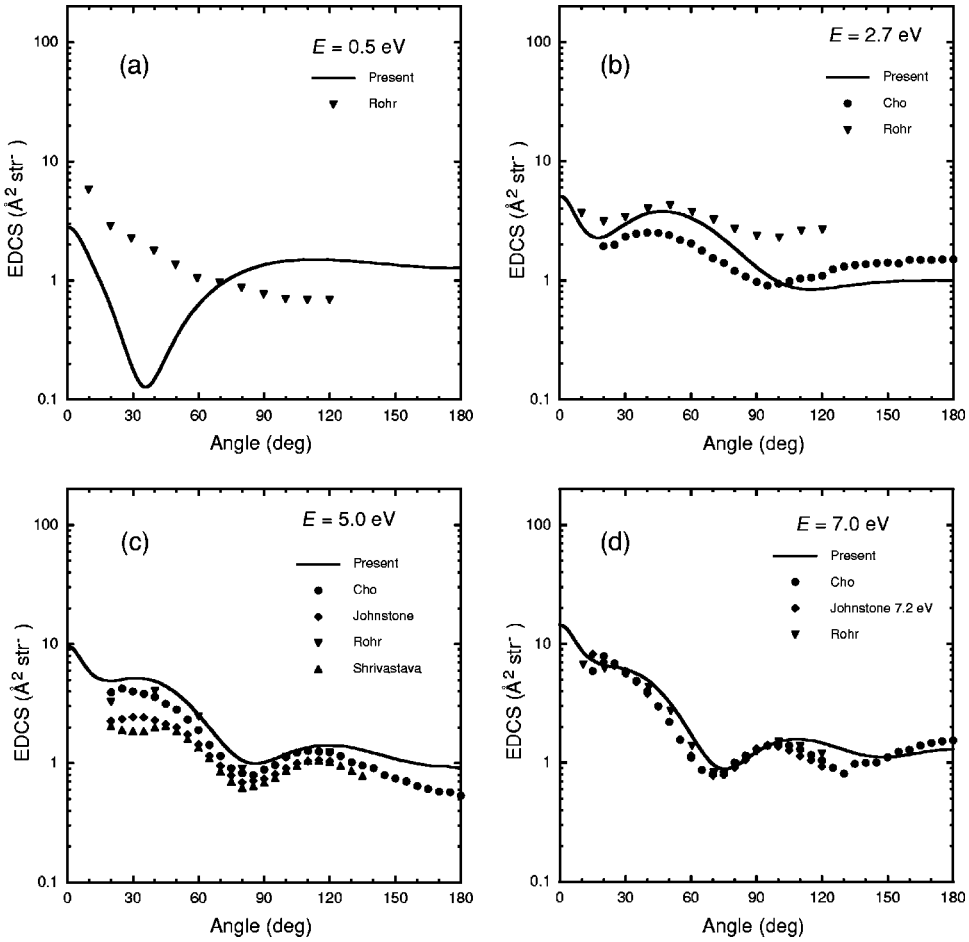

FIG. 3. Comparison between computed and measured DCS values at four different collision energies. The solid lines show the present calculations. The experiments are: Rohr from Ref. 17; Cho from Refs. 5 and 6; Johnstone from Ref. 16; Shrivastava from Ref. 18.

The low-energy A_{1g} resonance is a special case, however, as we can see from its behavior shown in Table II. Our earlier work[7] located it at 3.299 eV with a width of 0.032 eV (there is a typographical error in Table I of Ref. 7) using $l_{\max}=30$ and the 6-311G$(2p,2d)$ basis mentioned above. The present calculations with the different basis sets change both values much more than for the other resonances: The QZ results appear to have now converged but differ from the earlier ones by more than expected. Furthermore, if we vary the $l_{\max}$ value of the partial wave expansion, thereby changing the number of coupled equations, we see (at the bottom of Table II) that both E_R and Γ_R change rather markedly. A qualitative understanding for such a behavior could be had if we report the actual shape of the partial cross section of A_{1g} symmetry over the region of the resonance and as a function of $l_{\max}$, using only the QZ expansion. The results are given in Fig. 2 and tell us the following:

(i) The A_{1g} resonance in this energy region appears to be a ''window'' shape resonance for some values of $l_{\max}$ over a strongly changing background scattering rather than causing an overall enlargement of the partial integral cross section as in the other instances.[7]

(ii) Because of the strong dependence of the background contribution on collision energy (and, from Fig. 2, also on the partial-wave expansion) the usual quadratic fit of the corresponding phase shift

$$\delta_{\text{background}}=a+bE+cE^2 \tag{7}$$

becomes very sensitive to the cross section shape and therefore markedly modifies the results of the resonant contribution, δ_R, obtained by using the usual Breit–Wigner formula for isolated resonances.[7] On the whole, however, we feel that also in this special case, the resonance features given by $l_{\max}=40$ and with the QZ basis set expansion provide a reasonably converged result, as indicated by the data of Table II.

All the present calculations for angular distributions and integral cross sections were therefore carried out using the QZ basis set for the target orbitals and $l_{\max}=40$ as the largest contributing partial wave for the continuum electron.

IV. ELASTIC SCATTERING ANGULAR DISTRIBUTIONS

As mentioned earlier, the shape and values of the angular distributions of the scattered electron in the molecular gas obtained from a theoretical treatment provide a rather stringent test on the reliability of the calculations once they can be compared with experimental data on an absolute scale. In the case of the SF_6 molecule such data indeed exist from several experimental laboratories and they turn out to still differ from each other.

In particular, the most recent experiments which stem from the Australian group of Buckman and co-workers[5,6] and will be labeled as ''Cho'' in the following figures. Earlier data had been obtained at some energies by Johnstone and

Downloaded 06 Jan 2009 to 143.248.103.32. Redistribution subject to AIP license or copyright; see http://jcp.aip.org/jcp/copyright.jsp

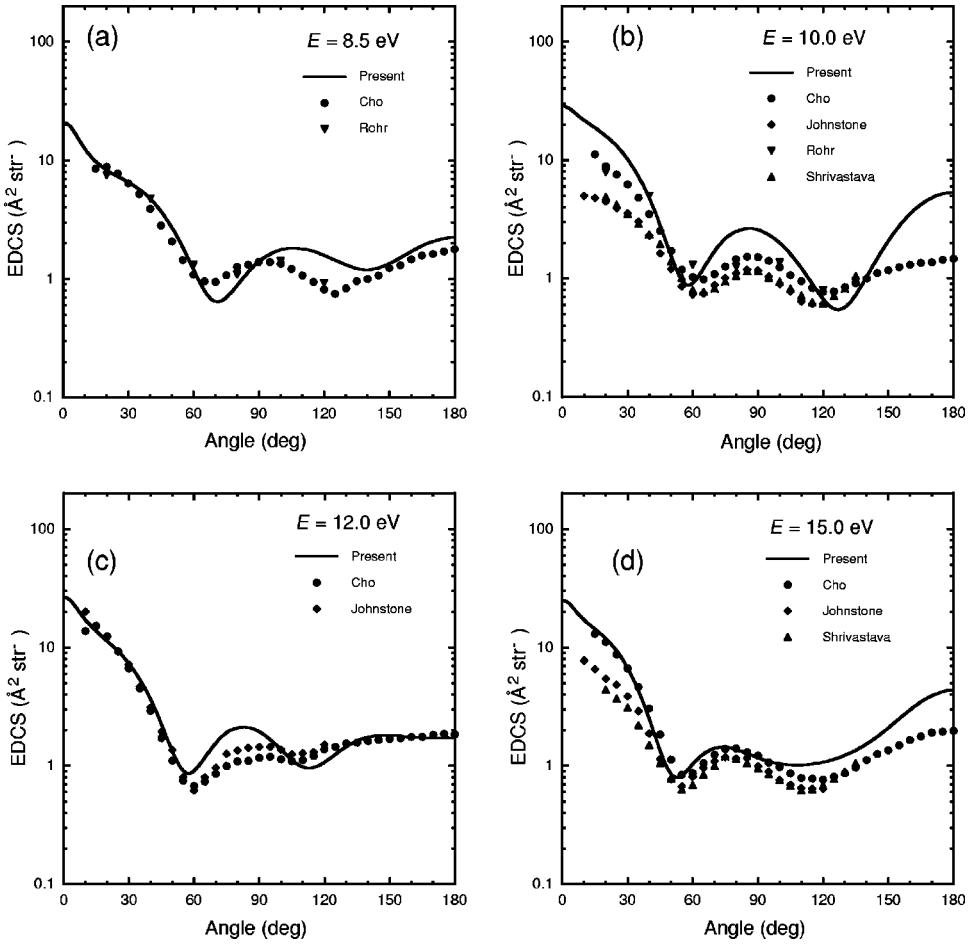

FIG. 4. Same as in Fig. 3 but for four different values of collision energies. (a) 8.5 eV; (b) 10 eV; (c) 12 eV; (d) 15 eV.

Newell[16] the data from which will be labeled below as ''Johnstone.'' Earlier measurements were provided by the Kaiserslautern group[17] and will be labeled as the ''Rohr'' data in our figures. Even earlier angular distributions were given by Trajmar's group[18] and will be labeled below as ''Srivastava.'' Finally, further data at a few higher energies come from a Japanese group[19] and will be labeled as ''Sakae'' in our figure.

The lowest four collision energies for which the experimental data are available are shown in the four panels of Fig. 3, from 0.5 eV (upper left panel) to 7.0 eV (lower right panel). It is interesting to note that our calculations follow very closely the experimental data of Refs. 5 and 6, which are the latest data and are given on an absolute scale, and do so at the three energies available. At 2.7 and 5.0 eV all the other experimental data are fairly different from Cho's data (which are considered the most accurate[5,6]) and our calculations confirm the Cho's values at both energies and also at 7.0 eV. The only available data at very low energies (0.5 eV) are those produced by Rohr. The comparison shows that they differ markedly from our calculations in the small-angle region. However, without any other experimental comparison, it is hard to say which values are the more reliable ones.

Figures 4 and 5 further report comparisons with experimental data for energies from 8.5 eV up to 50.0 eV, for a range of eight different values. Here again our calculations appear to follow fairly closely the shapes and values of the experimental data of Cho *et al.*[5,6] Our theory provides good accord in the forward scattering region, it confirms the presence of one or more minima at specific angles which vary slowly as the energy increases, and shows larger differences in the backward scattering region, generally suggesting the correct DCS shapes but indicating larger intensity values. The two highest collision energies for which we were able to find experimental data are reported in Fig. 6, where DCS at 60.0 eV and 75.0 eV are shown.

Once more we see there that the computed shape of the angular distributions follows very closely the one given by the experiments, although our computed values suggest larger intensities at the highest energy. On the whole, however, considering that we have evaluated angular distributions for elastic scattering without any empirical adjustment and that we were able to agree fairly well with experiments from about 2.7 to 75 eV of collision energy, one can consider the present SECP quantum treatment of the scattering events as a realistic description of the physics involved. Its computational demand is also fairly contained if we consider that the present level of computation requires for one energy value and for the full angular range of a set of DCS points about 1.0 h of CPU time for orbital expansion, 35.7 h for the scattering calculations at one energy for all symmetries and 10.6 h to compute the DCS values. The employed workstation here was an SGI R10000 running at 200 MHz.

Downloaded 06 Jan 2009 to 143.248.103.32. Redistribution subject to AIP license or copyright; see http://jcp.aip.org/jcp/copyright.jsp

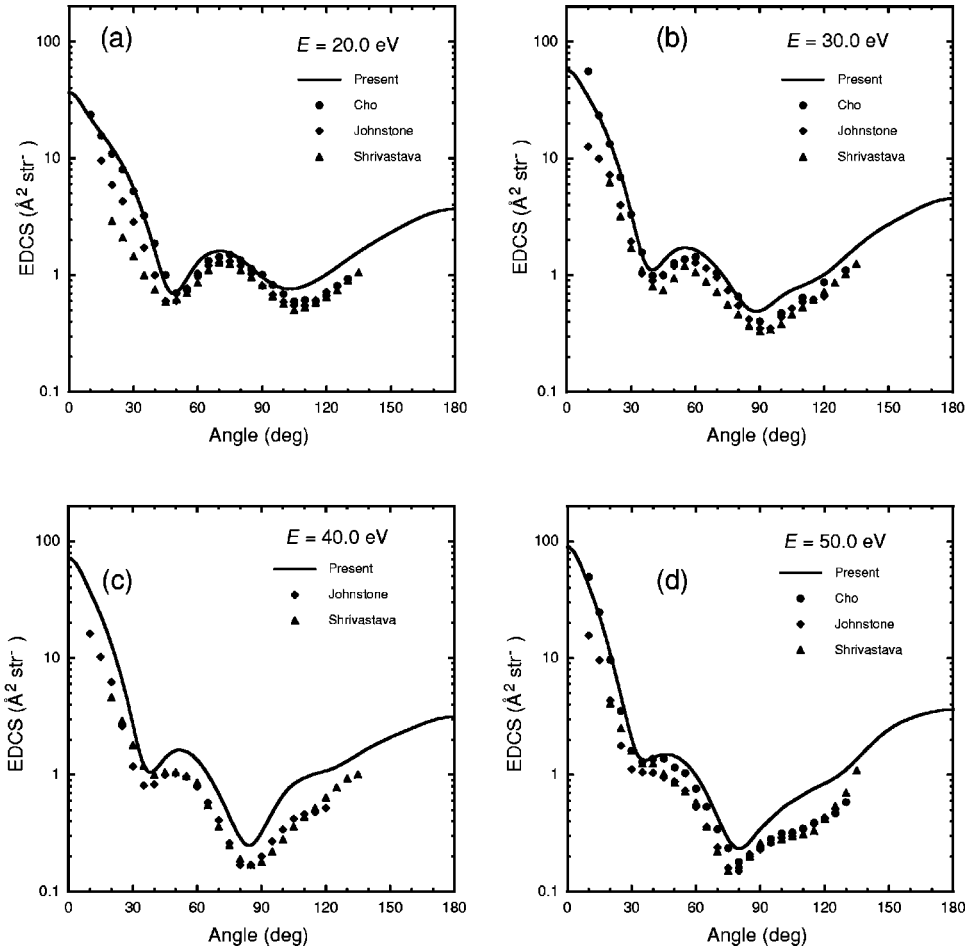

FIG. 5. Same as in Figs. 3 and 4 but for four different values of collision energies. (a) 20 eV; (b) 30 eV; (c) 40 eV; (d) 50 eV.

V. ELASTIC, TOTAL, AND MOMENTUM TRANSFER CROSS SECTIONS

The experiments that carried out the angular distribution measurements also provided the corresponding elastic cross sections (ECS) and total cross sections (TCS) by angular integration. Further data exist for the above quantities alone and were published by Dababneh *et al.*,[20] who published both TCS and the momentum-transfer cross sections (MTCS). They are reported as ''Dababneh'' in our following figures. The same quantities had also been published earlier on by Kennerly *et al.*[21] and will be labeled as ''Kennerly'' in our figures. The latest measurements for TCS were those by the Polish group[22] and will be labeled as ''Kasperski'' in our figures below. The total cross sections were also measured by Ferch *et al.*,[23] by Zecca *et al.*,[24] and by Randell *et al.*,[25] while the vibrational excitation cross sections were given by Rohr.[26]

The comparison of all the experimental data was done fairly comprehensively in a recent study,[27] where the presence of substantial discrepancies between the existing measurements over the various energy regions was pointed out in detail. The latest data[5,6] on the ECS predict values that are

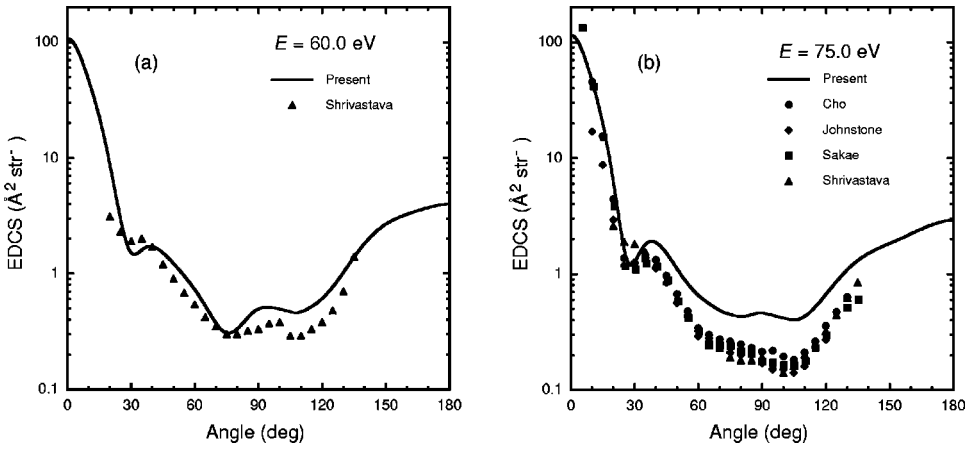

FIG. 6. Same as in Figs. 3, 4, and 5 but for the highest two collision energy values. (a) 60 eV; (b) 75 eV. The experiments marked Sakae are from Ref. 19.

Downloaded 06 Jan 2009 to 143.248.103.32. Redistribution subject to AIP license or copyright; see http://jcp.aip.org/jcp/copyright.jsp

TABLE III. Computed elastic integral cross sections (ECS) and momentum transfer cross sections (MTCS) in comparison with the experiments from Refs. 5 and 6. Computed results were obtained using the QZ basis set and using $l_{max}=40$.

	Present results		Experiments (from Refs. 5 and 6)	
Energy (eV)	ECS (Å^2)	MTCS (Å^2)	ECS (Å^2)±20%	MTCS (Å^2)±20%
2.7	23.427	16.608	18.73	16.10
5.0	26.071	17.763	20.15	14.14
7.0	26.842	17.976	24.29	15.47
8.5	28.380	19.373	24.60	14.49
10.0	37.764	23.002	24.45	15.09
12.0	30.501	19.951	26.81	17.62
15.0	27.892	19.211	25.51	14.86
20.0	27.750	18.768	24.73	15.65
30.0	29.397	18.924	29.72	13.18
50.0	26.415	15.086	22.13	8.09
75.0	24.230	12.557	18.02	7.28

substantially higher than all the previous ones and therefore a smaller presence of inelastic processes at low energy.

In Table III we report for comparison our computed values of ECS and MTCS, at the energies measured by the most recent experiments,[5,6] together with the actual experimental values quoted there. All the calculations were carried out using the QZ expansion and $l_{max}=40$ for the partial-wave expansion of the continuum electron. Our computed values for the ECS present a trend with energy which is fairly close to the experimental data, as is also shown pictorially by the right-hand side panel of Fig. 7, where all the available experimental points are shown. Given the fact that the experimental values are attributed an uncertainty of ±20% in Refs. 5 and 6, we see that our calculations fall on average very close within that uncertainty and always on the upper range of the values. The behavior is even better for the case of the MTCS, where the same uncertainty is considered in the experiments,[5,6] and for which our calculations fall, especially in the lower energy range, within the experimental error bars. Considering the complexity of the system, and the quality of the recent experiments, we can consider the present SECP modeling of the electron–molecule forces, and our quantum treatment of the dynamics, as indeed providing a realistic rendition of the process at hand.

Figure 7 reports the energy dependence of our computed ECS in comparison with both the experimental elastic cross sections (right-hand panel) and the experimental total cross sections (left-hand panel). We wanted to show there the overall energy dependence and we have therefore used a linear energy scale from ~0 eV and up to 100 eV. The comparison shows clearly that the computed ECS values strongly favor the latest measurements of Cho *et al.*,[5,6] while all previous data turn out to be substantially smaller. The same comparison with the total cross section data correctly finds most of them to lay above our computed ECS, with the exceptions of the Kennerly data[21] which, below ~30 eV, stay below our calculations and are the smallest of all the measured total cross sections.

The low-energy range of both sets of integral cross sections is shown by Fig. 8, where we present, on an enlarged log scale, the computed and measured ECS (right-hand panel) and TCS (left-hand panel). We are also reporting Rohr's extrapolation of the ECS at low energies.[17] The experimental TCS below 2 eV of collision energy show in all experiments a marked increase that should be chiefly driven there by the $-1/r^4$ polarization potential and by the dominance of the *s*-wave scattering at such low energies.[25] The fact that our computations are still fairly flat in the same region indicates that the inelastic components of the experimental TCS are likely to contain contributions from the *s*-wave vibrational excitation channel in the A_{1g} mode[25] that are not present in the elastic channel of our calculations. A further example of the low-energy behavior of the cross sections is shown in Fig. 9, which reports the same results as in Fig. 8 but on a larger energy scale now extended down to the millielectronvolts range.

What we now see in both panels is the presence of a strong increase of our computed ECS, as the collision energy decreases, showing up at much lower energies than those exhibited by the experimental TCS data. Thus, the calculation confirms a strong *s*-wave dominance in the very-low energy region as surmised by the experiments,[25] where however the likely presence of vibrational excitation effects guided by the large dipole polarizability of the title system shift that minimum from around the 60 meV position of the elastic channel to about 1000 meV. Here again the details of

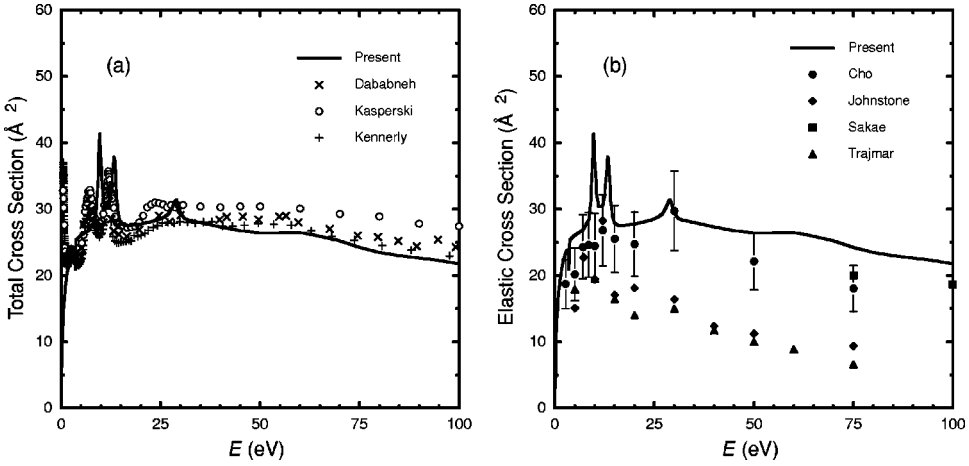

FIG. 7. Comparison between computed ECS and measured ECS and TCS. The energy scale is linear and covers from ~0 eV up to 100 eV. (a) TCS comparison; (b) ECS comparison. The experiments are: Dababneh from Ref. 20; Kennerly from Ref. 21; Kasperski from Ref. 22; Trajmar from Ref. 28.

Downloaded 06 Jan 2009 to 143.248.103.32. Redistribution subject to AIP license or copyright; see http://jcp.aip.org/jcp/copyright.jsp

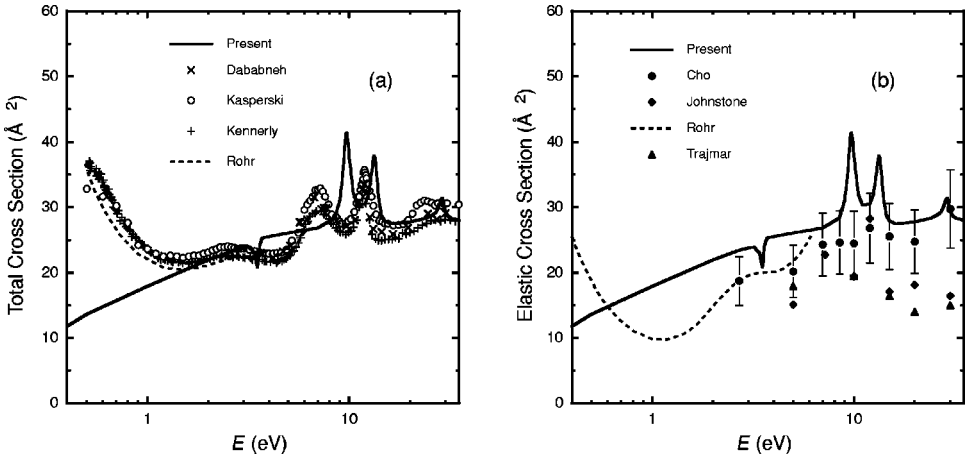

FIG. 8. Same as in Fig. 7 but on a log energy scale up to 30 eV.

the long-range interaction and the additional effects from contributing inelastic channels to the dominant $l=0$ component of the threshold scattering are changing the total cross section behavior from that of the elastic channel alone, where experiments however do not reach such low energy values and therefore our calculations provide the only comparison. We will not further analyze the strong resonance features that appear in the energy region around 10 eV because we have already done so in our previous studies.[7,29]

Figure 10 reports comparisons between the computed MTCS and the available experiments: The left-hand panel shows, on a log scale, the low-energy-behavior of this quantity while the right-hand panel shows the same values but on a linear scale of energy going up to 100 eV.

At the low collision energies, the behavior of the MTCS from our calculations follow very well the values given by the experiments, as we have already discussed in Table III. However, for energies above ~20 eV, we see that our calculations become larger and remain so all the way out to 100 eV. Since the MTCS weights more heavily, in its convolution process of the DCS, the values of the angular distributions which correspond to large-angle scattering and to the backscattering region (where $\cos\theta_{CM}$ approaches -1) then the present comparison suggests that our computed DCS values, as discussed in the previous section, become markedly larger than the experiments in the large-angle, high-energy regions of the process.

The presence of the marked cross section increase in the low energy dependence of the MTCS is further underlined in the panels of Fig. 11. The one on the right-hand side shows, on a logarithmic scale, the dependence of our computed values in the very low energy region where they clearly repeat the strong intensity drop of the cross sections around 60 meV, as did the computed ECS shown before. In fact, the left-hand panel of the same figure reports the superposition of our two computed sets of values on the same energy range of the previous panel. One clearly sees there that all the features exhibited by the integral cross sections in the low energy range are also present, as expected, in the MTCS. Both observables were of course obtained from the same set of *K*-matrix scattering calculations but were processed differently. The fact that they come out to behave so similarly is a further check of the correctness of our procedure.

VI. SUMMARY AND CONCLUSIONS

In the present work we have carried out, using different basis set expansions to describe the electronic state of the target molecular gas, electron scattering calculations for the e-SF_6 system from a few meV of collision energy up to about 100 eV. The computation yields elastic angular distributions of the scattered electrons over several values of collision energies. All the obtained DCS have been compared with existing experiments and the agreement shown by our

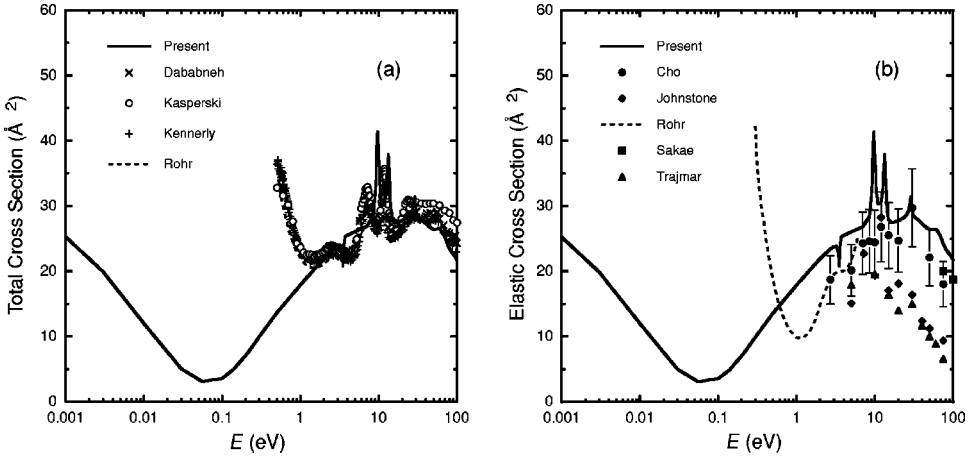

FIG. 9. Same as in Figs. 7 and 8 but on a log energy scale covering five orders of magnitude.

Downloaded 06 Jan 2009 to 143.248.103.32. Redistribution subject to AIP license or copyright; see http://jcp.aip.org/jcp/copyright.jsp

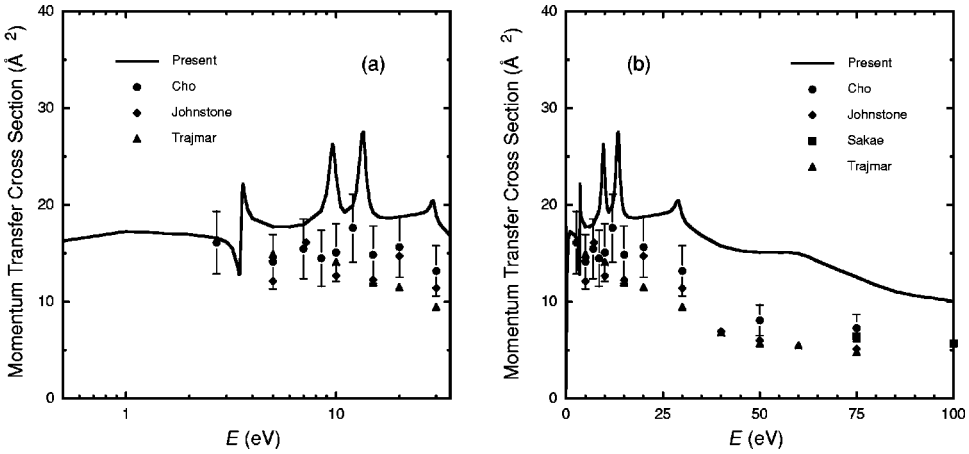

FIG. 10. Comparison between computed and measured momentum transfer cross sections as a function of collision energy. The left panel (a) shows the data on a log scale from 0.1 eV up to 30 eV. The right panel (b) shows a linear energy scale from about 0 eV up to 100 eV.

computed values with these data has been excellent at all energies, excluding the lowest one (see Fig. 3).

We have also computed the corresponding elastic integral cross sections (ECS), have compared them with the latest experimental values[5,6] and also with the existing data for the grand total integral cross sections (TCS). The comparisons over various ranges of collision energy have shown the following:

(i) The latest experimental data[5,6] produce the largest values for the ECS and our calculations are then within the upper error bars of these measurements, while being larger than the earlier experimental data. Our calculations therefore support the findings from the measurements of Refs. 5 and 6.

(ii) All the TCS data from the experiments are, as one should expect, larger than our computed elastic cross sections, especially above 30–40 eV, where the inelastic contributions are known to become more important. One exception is given by the measurements of Ref. 20, which are smaller than our ECS below about 30 eV.

(iii) The computations indicate that our results are essentially converged within 1%–2% when using the QZ basis set expansion and the $l_{\max}=40$ partial wave expansion for the continuum electron. They also reproduce the same strong resonant features around the region of 10 eV as shown by our earlier work.[7]

(iv) The very low-energy A_{1g} shape resonance, appearing against a background scattering that strongly depends on collision energy, is shown to be a ''window'' resonance whose features (position and width) are strongly affected by the convergence parameters that we have tested in this work.

(v) At very low energy our computed ECS and MTCS values are seen to markedly increase as the energy decreases down to around 60 meV. The TCS data from experiments indicate a similar effect that is however shifted up to around 1000 meV due to the influence of inelastic channels, as discussed earlier.[25]

(vi) The computed MTCS are in very good agreement with the experimental values in the range from 2 to about 25 eV, while they are larger than the experimental data at higher energies up to 100 eV. They never became, however, more than 50% larger than the measurements, indicating that the large-angle experimental DCS that are still usually missing,[5,6] would provide an essential datum for this comparison.

In conclusion, the present study of the scattering features of the e-SF_6 system and the comparison of them with the available experiments have shown our theoretical method to be physically reliable, computationally robust and with still acceptable demands on CPU time. It describes several dynamical attributes of the scattering process and gives them in

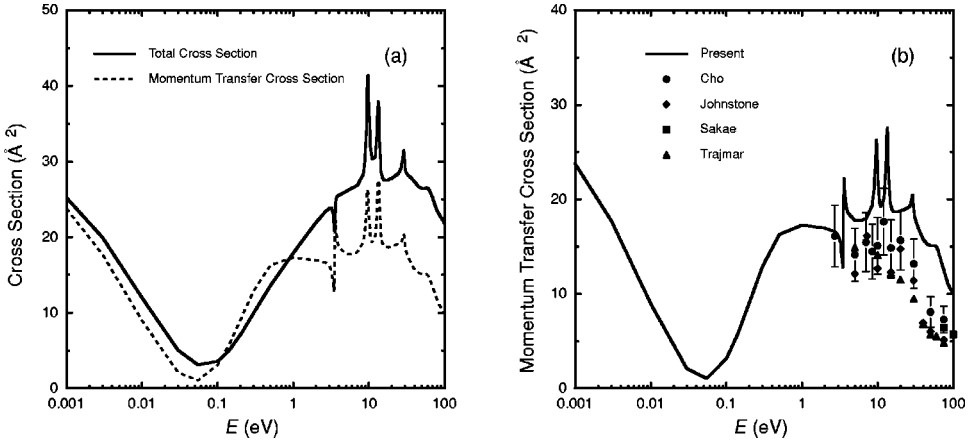

FIG. 11. Same as in Fig. 10 but on a log energy scale covering five orders of magnitude. Left panel (a): comparing the present computed values for the elastic total cross section and the momentum-transfer cross section. Right panel (b): comparing computed and measured momentum-transfer cross sections. The labeling of the experimental data is the same as in the previous figures.

Downloaded 06 Jan 2009 to 143.248.103.32. Redistribution subject to AIP license or copyright; see http://jcp.aip.org/jcp/copyright.jsp

fairly good accord with measurements, providing a realistic theoretical and computational framework for the study of elastic channel behavior in large, polyatomic gases.

ACKNOWLEDGMENTS

The financial support of the Italian National Research Council (CNR) and of the Italian Ministry for University and Research (MURST) is gratefully acknowledged. One of us (R.R.L.) thanks the Welch Foundation for financial support through Grant No. A-1020. The support of the Texas A&M University Supercomputing Facility is also acknowledged. We also thank the NATO Research Division for the award of Collaborative Research Grant No. 922/94/JARC501 during the tenure of which this work was carried out. We are grateful to Professor Buckman for letting us have several details about his measurements and some unpublished data. Finally, F.A.G. thanks the Max-Planck Society for financial support and the Institut for Strömungsforschung in Göttingen for its hospitality during the completion of the present work.

[1] For example, see, *Plasma Processing of Materials* (National Academic Press, Washington, DC, 1991).
[2] J. N. Bardley, in *Abstracts of the International Conference on Atomic and Molecular Data and Their Applications*, edited by W. L. Wiese (NIST, Washington, DC, 1997), p. 3.
[3] For example, see, L. G. Christophorou, J. K. Olthoff, and M. V. V. S. Rao, J. Phys. Chem. Ref. Data **26**, 1 (1997).
[4] For a recent review of methods, see *Computational Methods for Electron–Molecule Collisions*, edited by W. H. Huo and F. A. Gianturco (Plenum, New York, 1995).
[5] H. Cho, R. J. Gulley, and S. J. Buckman, J. Phys. B **33**, L309 (2000).
[6] H. Cho, R. J. Gulley, K. W. Trantham *et al.*, J. Phys. B **33**, 3531 (2000).
[7] For example, see F. A. Gianturco and R. R. Lucchese, J. Chem. Phys. **108**, 6144 (1998).
[8] F. A. Gianturco, R. R. Lucchese, and N. Sanna, J. Chem. Phys. **102**, 5743 (1995).
[9] F. A. Gianturco and A. Jain, Phys. Rep. **143**, 347 (1986).
[10] For details, see F. A. Gianturco and N. Sanna, Comput. Phys. Commun. **114**, 142 (1999).
[11] M. H. F. Bettega, C. Winstead, and V. McKoy, J. Chem. Phys. **112**, 8806 (2000).
[12] For example, see R. G. Parr and W. Yang, *Density Functional Theory of Atoms and Molecules* (Oxford University Press, Oxford, 1989).
[13] F. A. Gianturco, R. R. Lucchese, and N. Sanna, J. Chem. Phys. **100**, 6464 (1994); **104**, 6482 (1996).
[14] F. A. Gianturco and R. R. Lucchese, J. Chem. Phys. **111**, 6769 (1999).
[15] A. P. P. Natalense and R. R. Lucchese, J. Chem. Phys. **111**, 5344 (1999).
[16] W. M. Johnstone and W. R. Newell, J. Phys. B **24**, 473 (1991).
[17] K. Rohr, J. Phys. B **12**, L185 (1979).
[18] S. K. Srivastava, S. Trajmar, A. Chutjian, and W. Williams, J. Chem. Phys. **64**, 2767 (1976).
[19] T. Sakae, S. Sumiyoshi, E. Murakami *et al.*, J. Phys. B **22**, 1385 (1989).
[20] M. S. Dababneh, Y.-F. Hsieh, W. E. Kauppila *et al.*, Phys. Rev. A **38**, 1207 (1988).
[21] R. E. Kennerly, R. A. Bonham, and M. McMillan, J. Chem. Phys. **70**, 2039 (1979).
[22] G. Kasperski, P. Mozejko, and C. Szmytkowsky, Z. Phys. D: At., Mol. Clusters **42**, 187 (1997).
[23] J. Ferch, W. Raith, and K. Schröder, J. Phys. B **15**, L175 (1982).
[24] A. Zecca, G. Karwasz, and R. S. Brusa, Chem. Phys. Lett. **199**, 423 (1992).
[25] J. Randell, D. Field, S. L. Lunt *et al.*, J. Phys. B **25**, 2899 (1992).
[26] K. Rohr, J. Phys. B **10**, 1175 (1977).
[27] L. Christophorou, J. Olthoff, R. Siegel *et al.*, Bull. Am. Phys. Soc. **44**, 20 (1999).
[28] S. Trajmar, D. F. Register, and A. Chutjian, Phys. Rep. **97**, 219 (1983).
[29] R. R. Lucchese and F. A. Gianturco, Int. Rev. Phys. Chem. **115**, 429 (1996).

Downloaded 06 Jan 2009 to 143.248.103.32. Redistribution subject to AIP license or copyright; see http://jcp.aip.org/jcp/copyright.jsp